Limnol. Oceanogr., 55(3), 2010, 1338–1352

doi:10.4319/lo.2010.55.3.1338

Role of sulfate reduction and methane production by organic carbon degradation in eutrophic fjord sediments (Limfjorden, Denmark)

Bo Barker Jørgensen[1,2,*] and R. John Parkes[3]

Department of Biological Sciences, Ny Munkegade, Aarhus University, Århus, Denmark

Abstract

The anaerobic mineralization of buried organic matter through sulfate reduction and methanogenesis was studied in 2-m-long piston cores of organic-rich, silty-clay sediment from two sites in Limfjorden, Denmark. An extended sulfate–methane transition (SMT) zone was found at 1–1.5-m sediment depth, accompanied by peaks in sulfide (4–6 mmol L^{-1}) and high dissolved inorganic carbon (30–50 mmol L^{-1}). Pore-water acetate concentrations were 2–10 μmol L^{-1}. ^{14}C-acetate was oxidized to $^{14}CO_2$ in the sulfate zone and reduced to $^{14}CH_4$ at and below the SMT. CO_2 reduction was the predominant pathway of methanogenesis below the sulfate zone. Sulfate reduction rates (SRRs) determined by ^{35}S tracer experiments decreased with depth throughout the sulfate zone from $>$ 100 nmol cm^{-3} d^{-1} near the sediment surface to $<$ 1 nmol cm^{-3} d^{-1} at depth. The depth trend of rates was equally well described by a power law function and a reactive continuum model. Only a small percentage of the total ^{35}S-SRR was due to anaerobic oxidation of methane. In contrast, diffusion–reaction modeling of pore-water sulfate indicated that sulfate reduction was insignificant throughout the sulfate zone and that most of the activity occurred at the SMT. A comparison of the burial flux of organic carbon below the sulfate zone and the returning flux of methane indicated that the diffusion modeling of pore-water sulfate strongly underestimated in situ SRRs, whereas the ^{35}S data may have overestimated the rates at depth. Modeled and measured SRR could be reconciled provided that bioirrigation reached to at least 20–40-cm sediment depth, which appears realistic given the predominant burrowing polychaete fauna.

Fine-grained sediments with a high content of organic matter, which accumulate in protected, eutrophic estuaries and embayments, are generally highly reducing and sulfidic beneath a few-centimeters-thick oxic and/or oxidized surface layer. The deposited organic matter, which escapes aerobic mineralization, is therefore effectively buried in the zone dominated by bacterial sulfate reduction. A much smaller fraction of the buried organic matter remains to be degraded below the one- to several-meters-deep sulfate zone, at depths where methanogenesis is the terminal pathway of organic carbon mineralization.

Several factors control the proportion of the deposited organic matter that is converted into methane beneath the sulfate zone. Pore-water sulfate profiles often show nearly linear gradients down to the sulfate–methane transition (SMT), indicating little sulfate consumption within the entire sulfate zone (Borowski et al. 1999). Consequently, diffusive transport-reaction models of pore-water sulfate tend to conclude that a large part of the sulfate reduction is driven by the anaerobic oxidation of methane (AOM) at the bottom of the sulfate zone (Borowski et al. 1996). In contrast, experimental measurements of sulfate reduction using ^{35}S-labeled sulfate consistently show high rates near the sediment surface, with rates decreasing only gradually down towards the SMT (Jørgensen et al. 2001).

In the present study we analyzed the balance between carbon burial, sulfate reduction, and methane cycling in organic-rich sediments of Limfjorden, using sediment stations at which the sulfur cycle had been previously studied (Jørgensen 1977). By combining radiotracer experiments and pore-water modeling we tried to reconcile mineralization rates via sulfate reduction or methanogenesis as determined from the two approaches. Specifically, we used estimated burial fluxes of total organic matter and upwards fluxes of methane to constrain a power law model that describes organic carbon mineralization rates as a function of sediment depth and age. Information about the Holocene geological development of the sediments was used to constrain these estimates.

Methods

Limfjorden is a shallow, eutrophic sound in northern Denmark connecting the North Sea in the west to the Kattegat in the east. The central part consists of branching straits and broads with salinities varying between 20 and 30. During the late Holocene, the connection to the North Sea changed repeatedly, as witnessed by the alternating predominance of marine or brackish benthic fauna and phytoplankton down through sediment cores (Kristensen et al. 1995; Christensen et al. 2004).

Two sites were sampled during August 1987, at the positions given in Table 1 (Fig. 1). Sta. 3 in Bjørnsholm Bay and Sta. 2 in Livø Strait are situated in the central part of Limfjorden at 10- and 7-m water depth, respectively. The station numbers are according to Jørgensen (1977). At the

* Corresponding author: bo.barker@biology.au.dk

Present addresses:
[1] Max Planck Institute for Marine Microbiology, Bremen, Germany
[2] Center for Geomicrobiology, Department of Biological Sciences, Aarhus University, Århus, Denmark
[3] School of Earth and Ocean Sciences, University of Cardiff, Cardiff, United Kingdom

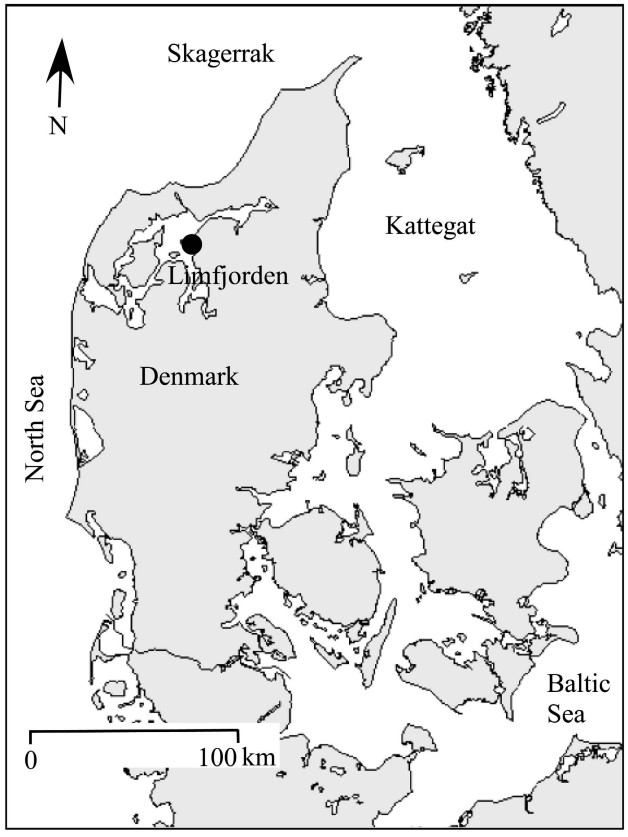

Fig. 1. Map of Denmark with Limfjorden. The sampling sites in Bjørnsholm Bay and Livø Strait are covered by the filled circle.

time of sampling, the bottom water temperature was 16°C and the salinity was 20–22 (Table 1). The mean annual temperature in Limfjorden is ca. 9°C. Temperatures in the sediment measured immediately on freshly retrieved cores from Sta. 3 were 0-cm depth, 15.7°C; 1.7-m depth, 12.1°C; and 2.7-m depth, 9.9°C. The two stations have been described earlier with respect to general sediment properties, sulfur biogeochemistry, and Holocene history (Jørgensen 1977; Christensen et al. 2004).

Sampling was done from the R/V *Genetica* of Aarhus University. Sediment cores of 9-cm diameter and ca. 300-cm length were taken by a piston corer constructed by Niels Iversen. In order to obtain intact surface sediment, additional 15-cm-deep cores were taken by a Haps corer (Kanneworff and Nicolaisen 1973). The Haps cores were subcored on deck immediately after sampling, whereas the whole piston cores were transported immediately to the laboratory.

All cores were brought to the Rønbjerg Marine Station (Aarhus University) near Livø Strait in Limfjorden and placed upright in a thermostated room at 13°C within a few hours of sampling. This temperature was within ± 1°C of the in situ temperature at the SMT of Sta. 3 and Sta. 2 cores at the time of sampling. The piston cores were subcored on the day of sampling using core liners of 3.6 cm i.d. for pore water and 2.6 cm i.d. for all other parameters. The piston core was extruded at 15-cm increments using a large piston and

Table 1. Coring stations in Limfjorden, including depth, temperature, and salinity of the overlying water at the time of sampling.

Station	3. Bjørnsholm Bay	2. Livø Strait
Position	56°50.31′N, 09°08.96′E	56°53.10′N, 09°07.95′E
Depth (m)	10	7
Temperature (°C)	16.2	15.8
Salinity	20.2	22.6

subcores were taken consecutively from the central part of the exposed end, thus minimizing air exposure and avoiding the smeared periphery of the core. Subcores were stoppered and kept at 13°C until further treatment.

Pore-water analyses—Pore water was squeezed under an N_2 atmosphere from 2–4-cm-thick sediment segments through a 0.45-μm membrane filter (Millipore; Reeburgh 1967). The first 1 mL was discarded. The next 3–4 mL was collected in a pre-weighed glass vial containing 2 mL of 2% $ZnCl_2$ (analytical grade in double-distilled water) in order to precipitate dissolved sulfide. This sample was used for the determination of sulfate and free sulfide. The remaining pore water was collected in a clean, precombusted glass vial and used for the other analyses. Pore water for acetate determination was obtained by centrifuging sediment sections under nitrogen gas and then filtering through combusted (350°C for 8 h) GFC filters (Whatman) before storing frozen in acid-washed crimp vials.

Free sulfide (H_2S plus HS^-, collectively called H_2S) was determined on the ZnS precipitate in the fixed pore-water samples using the methylene blue spectrophotometric method of Cline (1969). Dissolved inorganic carbon (DIC) was determined as described by Devol et al. (1984).

After centrifugation and removal of ZnS, sulfate was determined by non-suppressed ion chromatography (Waters IC with conductivity detector). A subsample was diluted 30–50-fold in double-distilled water and membrane filtered just before analysis. A positive blank was present in controls without pore water but with distilled water and $ZnCl_2$, diluted similarly to the samples. This blank corresponded to ca. 0.1 mmol L^{-1} SO_4^{2-} in the undiluted samples. A value of 0.1 mmol L^{-1} was therefore subtracted from all sulfate data.

Methane was determined in 1-mL sediment samples taken with cut-off syringes. The sediment was transferred immediately into 12-mL serum vials containing 4 mL of 2.5% NaOH, stoppered by butyl rubber stoppers, shaken, and left for a day for the methane to equilibrate with the headspace. Duplicate 0.5-mL headspace samples were analyzed on a gas chromatograph with a 2-m × 2-mm Poropac Q column and a flame ionization detector (FID). The carrier gas was N_2 at a flow rate of 20 mL min^{-1}. Peaks were quantified on an integrator and calibrated against standards.

Acetate was analyzed by ion chromatography as described by Parkes and Taylor (1983). Calibration was achieved with external standards (2.5–15 μmol L^{-1}, r = 0.996). Reagent blanks did not contain detectable acetate

concentrations and the mean recovery of added acetate standards to pore-water samples was 103%. The detection limit was ca. 1 μmol L^{-1}.

Process rate measurements using radiotracers—Rates of microbial transformations of sulfate, acetate, and bicarbonate were determined using the whole-core injection method (Jørgensen 1978*a*). Injections of tracer amounts of the respective radiolabeled substrates were done at multiple depths in 26-mm-i.d. subcores and the formation of radiolabeled products was analyzed after incubation at the in situ temperature.

Sulfate reduction rates (SRRs) were determined by injection of 2 μL carrier-free ^{35}S-sulfate solution containing 200 kBq (ca. 5 μCi) of radioactivity. The depth resolution was 2 cm in the upper ca. 25 cm of the core and in the SMT. The depth resolution outside of these intervals was 5–10 cm. After 12 h incubation at 13°C the cores were sectioned and 2-cm segments were fixed in weighed vials containing 10 mL of cold 5% Zn-acetate. The sediment was immediately slurried to inhibit bacterial activity and to fix the sulfides. The slurry was centrifuged and a 0.5-mL sample was taken from the supernatant for the determination of ^{35}S-sulfate radioactivity. The sediment was then washed twice with freshwater to remove most of the remaining ^{35}S-sulfate, thereby reducing the subsequent ^{35}S-H_2S blank that may develop during hot chromium distillation (Kallmeyer et al. 2004). Total chromium reducible sulfides were dissolved by boiling a weighed subsample for 40 min with 1 mol L^{-1} Cr^{2+} in 12 mol L^{-1} HCl (Zhabina and Volkov 1978; Canfield et al. 1986; Fossing and Jørgensen 1989). The evolved ^{35}S-H_2S was collected in two serial traps containing 10 mL 2% Zn-acetate plus a drop of antifoam. The radioactivities of sulfate and sulfide were determined by liquid scintillation counting. Sulfate concentrations were recalculated to sediment volume units using the porosity data. The SRRs were calculated according to Jørgensen (1978*a*).

Rates of CH_4 or CO_2 production from acetate were determined similarly to rates of sulfate reduction, except that 2 μL of [U-^{14}C] acetate (7.4 kBq, $\sim$ 0.2 μCi, Amersham International) was injected. After $\sim$ 12 h incubation the sediment cores were sectioned into glass jars with 10 mL of 2.5% NaOH, sealed, and shaken thoroughly to stop activity. $^{14}CH_4$ in the headspace of these vials was determined using a gas chromatograph with FID to oxidize the CH_4 to CO_2 and trapping the $^{14}CO_2$ from the exhaust gas in 5 mL of 0.4 N NaOH. The slurry was then washed with 10 mL of water into a distillation jar, 1 mL of antifoam was added, and the sample was acidified by 8 mL 4 mol L^{-1} H_2SO_4 in 1-mL amounts to liberate CO_2. Any $^{14}CO_2$ produced was flushed out of the jar headspace with N_2 at 25 mL min^{-1} for 35 min and into a scintillation vial with 10 mL 1 : 7 v/v ethanolamine : ethylene glycol monomethyl ether (Ansbæk and Blackburn 1980). Scintillation fluid was then added and the contents mixed before the radioactivity was counted on a scintillation counter. Calculation of rates of turnover of acetate to CH_4 or CO_2 followed that for sulfate reduction, except that no fractionation factor was used. Analysis of bicarbonate methanogenesis was similar to the above and was based on procedures previously described (Kuivila et al. 1989).

Other determinations—Porosity, density, and ignition loss were determined at depth intervals of 2 cm in the Haps cores and 5 cm in the piston cores. Core segments of defined volume were transferred to pre-weighed crucibles and the sediment weight was determined before and after drying at 105°C overnight. Porosity was determined from the water loss per volume of sediment upon drying. Organic matter was subsequently determined from the weight loss upon ignition of the dried sediment at 450°C overnight.

Modeling—Pore-water profiles of sulfate, methane, and dissolved sulfide were used for one-dimensional transport-reaction modeling of net rates of sulfate reduction, methane oxidation, and sulfide production. We used the modeling software, PROFILE, of Berg et al. (1998), assuming steady state and transport by molecular diffusion. The latter criterion was valid only in the deep part of the sulfate zone, including the SMT, and in the methanogenic sediment below. The PROFILE model divides the sediment into a number of discrete depth intervals and calculates those rates of production or consumption that provide optimal fits to the concentration data.

Boundary conditions were for sulfate, concentration and flux = 0 at the bottom of the sulfate zone; for methane, concentration and flux = 0 at the top of the methane zone; and for sulfide, measured values of H_2S at the top and bottom of the sulfide zone. Whole-sediment diffusion coefficients, D_s, were calculated from tabulated data for diffusion coefficients (Schulz 2006), using the empirical formula of Iversen and Jørgensen (1993):

$$D_s = D/(1 + 3(1 - \varphi)) \quad (1)$$

where φ is the sediment porosity. A smoothed depth profile of the porosity data was used for the calculations. Molecular diffusion coefficients, D, corrected to the measured in situ temperature of 13°C at the SMT, were $D_{sulfate} = 0.74 \times 10^{-5}$ cm^2 s^{-1}, $D_{sulfide} = 1.36 \times 10^{-5}$ cm^2 s^{-1}, $D_{methane} = 1.16 \times 10^{-5}$ cm^2 s^{-1}, and $D_{DIC} = 0.81 \times 10^{-5}$ cm^2 s^{-1}.

It should be noted that sediment accumulation was not considered in the model as this has no significant effect on the model results in Limfjorden sediments (Jørgensen 1978*b*).

Correction of core depths—Samples used for chemical analyses or process rate measurements were taken from several parallel cores, as indicated in the results. Although care was taken to repeatedly core at the same position, depths in the different cores needed to be correlated accurately. This was possible by comparing the methane profiles in each core. Thus, marker samples of methane were taken at 20-cm depth intervals from all cores and used to adjust depths in relation to the SMT. Furthermore, the subsurface depths of two distinct shell layers were used to check the depth alignments at Sta. 3. The data showed that the necessary depth corrections were in the range of 5–12 cm at the depth of the SMT.

Results

Sta. 3, Bjørnsholm Bay—Sulfate and methane in the pore water were measured in two gravity cores with similar results (Fig. 2A,B). Sulfate penetrated from a surface concentration of 15–16 mmol L^{-1} to near zero below a depth of 120 cm. Methane from deeper sediment layers diffused up along a steep gradient and penetrated up into the lower sulfate zone. This provided a methane sink that was focused in the main SMT at 80–120-cm depth. There was, however, also an extensive tailing of methane up through the entire sulfate zone at mean concentrations of 0.02 mmol L^{-1}. Even in the top 0–1 cm of sediment the methane concentration was 0.007–0.010 mmol L^{-1}.

Modeling of the sulfate and methane profiles, as indicated in Fig. 2A,B, assuming transport by molecular diffusion only, showed rather similar depth distributions of net SRRs and rates of AOM in the two cores (Fig. 2C). Because of the modeling approach used, rates were calculated and averaged for discrete depth intervals. In the upper part of the sulfate zone, above the SMT, the SRR was either uniformly very low (Core 1) or somewhat elevated in the uppermost part (Core 2). The SRR was again elevated, ca. 0.5 nmol cm^{-3} d^{-1}, in the SMT centered at 100-cm depth. According to the modeling, AOM rates were about 0.2 nmol cm^{-3} d^{-1}, which is less than half of the modeled SRR in the SMT. The AOM apparently took place slightly deeper than the SRR peak rates.

Free sulfide (H_2S) increased from zero near the sediment surface to peak concentrations of 4.5 mmol L^{-1} at 120-cm depth, i.e., right at the bottom of the sulfate zone (Fig. 2D). Below the SMT, sulfide concentrations decreased again with depth. DIC increased rather uniformly with depth to reach 50 mmol L^{-1} at 150-cm depth (Fig. 2E). The concentration of bulk organic matter in the sediment scattered mostly between 5% and 10% dry weight and was related to the varying contents of silt or fine sand (Fig. 2F).

Sulfate reduction was measured experimentally with ^{35}S tracer at high depth resolution throughout the sediment core. Figure 2G shows the combined data from cores 1 and 2. In the strongly bioturbated upper 5–8 cm of the sediment, rates reached a maximum of 147 nmol SO_4^{2-} cm^{-3} d^{-1}. Below 10 cm, the rates dropped steeply and uniformly, with only a small peak at 115–120-cm depth, coinciding with the SMT (Fig. 2G, insert). This peak of up to 8 nmol cm^{-3} d^{-1} is presumably due to AOM-driven sulfate reduction. When the same data are plotted on log-log scales, the depth trend of SRR becomes quasi-linear, as indicated by the linear correlation line shown in Fig. 2H. The correlation line, calculated with omission of the elevated AOM-driven SRR, corresponds to the following depth dependence of sulfate reduction:

$$\log \mathrm{SRR} = 3.37 - 1.69 \times \log z, \text{ or}$$

$$\mathrm{SRR} = 2320 \times z^{-1.69} \text{ nmol cm}^{-3} \text{ d}^{-1} \quad (2)$$

where z is the sediment depth in centimeters. At the bottom of the sulfate zone, the peak of AOM-driven SRR is visible in Fig. 2H.

The depth-integrated, cumulative sulfate reduction in Fig. 2I was calculated from the log-log linear correlation, starting at 5-cm depth. For the top 0–5 cm we used the mean rate for that interval, 95 nmol cm^{-3} d^{-1}. By this calculation the rates measured or calculated at each depth and expressed in nmol SO_4^{2-} cm^{-3} d^{-1} are compiled with depth to provide a stacked SRR under 1 cm^2 of sediment surface from the surface to depth z (unit nmol SO_4^{2-} cm^{-2} d^{-1}). The curve thus shows how large a fraction of the entire sulfate reduction took place from the sediment surface and down to a certain depth. For example, 75% of the total sulfate reduction in the sediment column took place in the top 0–20 cm and only 10% took place below 55 cm. The graph also shows that the measured AOM-driven SRR added only little to the total depth-integrated SRR, which was 1310 nmol cm^{-2} d^{-1} or 13.1 mmol m^{-2} d^{-1}.

Sta. 2, Livø Strait—Data from Livø Strait were rather similar to those from Bjørnsholm Bay. Sulfate penetrated slightly deeper, to 140 cm, and the methane showed similar tailing high up into the sulfate zone (Fig. 3A,B). Diffusion-reaction modeling indicated no net sulfate reduction in the upper 0–80 cm but distinct peaks of SRR of 0.2–0.5 nmol SO_4^{2-} cm^{-3} d^{-1} at the bottom of the sulfate zone (Fig. 3C). AOM peaked in the same zone but was again lower and showed a slight shift towards greater depth relative to the modeled SRR peaks. H_2S reached a maximum of 6 mmol L^{-1} at 125-cm depth (Fig. 3D) and DIC increased to 27 mmol L^{-1} at the bottom of the core (Fig. 3E). The bulk organic matter showed lower concentrations and less scattering than in Bjørnsholm Bay (Fig. 3F). SRRs dropped steeply below the sediment surface, and AOM-driven SRR could not be discerned (Fig. 3G). In a log-log plot, the SRR showed larger scatter than at Sta. 3 (Fig. 3H). A comparison of SRR data from this study and from a study done in 1977 (crosses in Fig. 3H; Jørgensen 1977) showed a similar degree of scatter in both data sets but no systematic difference. Linear correlation of the log-log plot indicated a general depth distribution of sulfate reduction according to

$$\mathrm{SRR} = 850 \times z^{-1.42} \text{ nmol cm}^{-3} \text{ d}^{-1} \quad (3)$$

Depth-integrated, cumulative rates of sulfate reduction showed a relative distribution similar to that in Bjørnsholm Bay (Fig. 3I), with a total areal rate of 1190 nmol cm^{-2} d^{-1} or 11.9 mmol m^{-2} d^{-1}.

Stoichiometry of mineralization—The net organic carbon mineralization to DIC was compared to the net sulfate reduction by plotting the pore-water concentration of DIC vs. sulfate at different sediment depths for both stations (Fig. 4A,B). The depth where sulfate showed tailing leading down into the methane zone was omitted from the plots because at that depth methanogenesis takes over as the main source of DIC production.

The results showed inverse linear correlations between the molar concentrations of DIC and sulfate, with slopes of −1.66 (r^2 = 0.94) for Bjørnsholm Bay and −1.19 (r^2 = 0.99) for Livø Strait. Because the sulfate diffuses down into

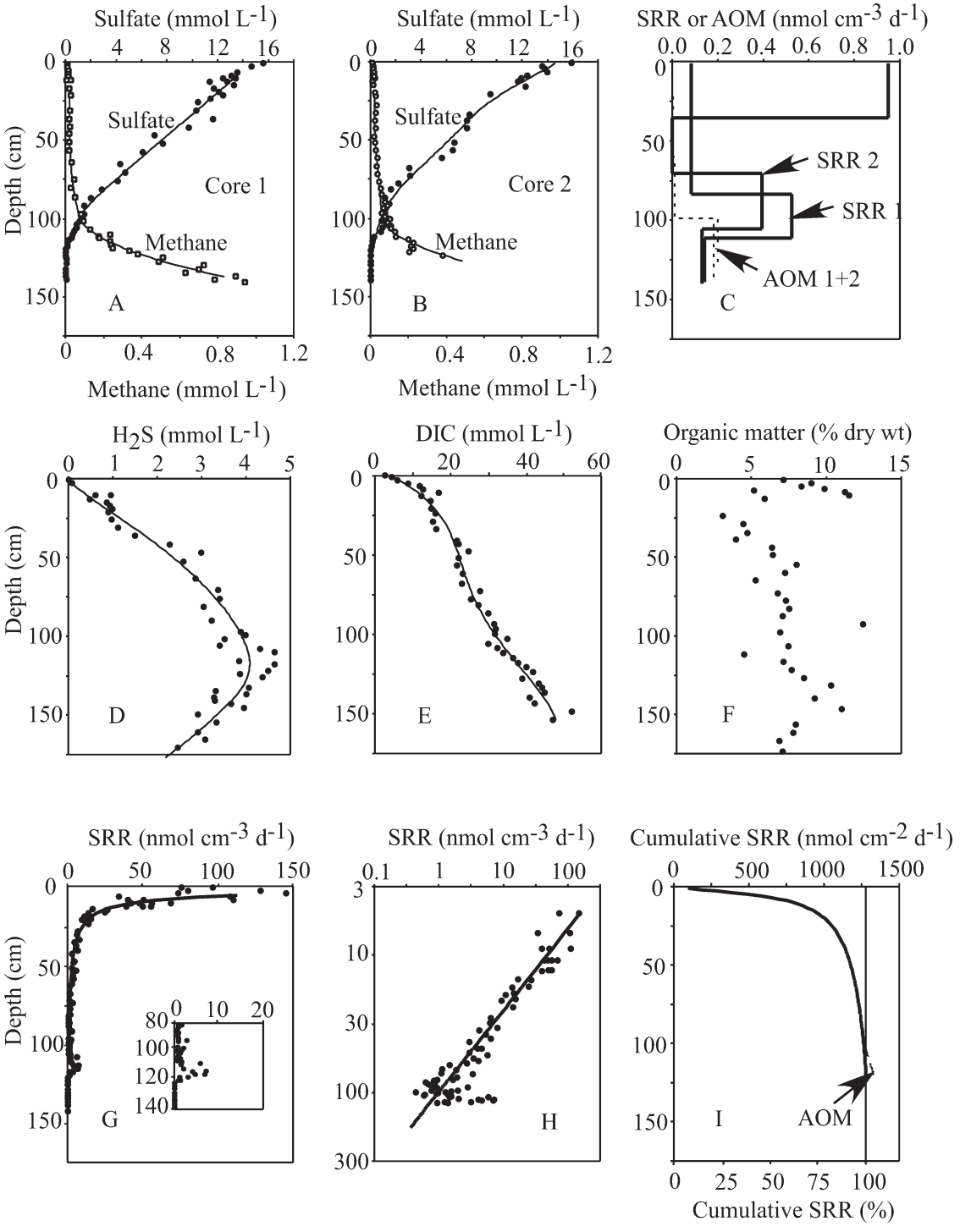

Fig. 2. Data from Sta. 3, Bjørnsholm Bay: (A, B) Sulfate and methane profiles in Cores 1 and 2, respectively; (C) modeled rates of sulfate reduction (SRR) and of anaerobic oxidation of methane (AOM) in Core 1 and Core 2; (D) dissolved sulfide (H_2S); (E) dissolved inorganic carbon (DIC); (F) total organic matter in the sediment; (G) sulfate reduction rates (SRR) measured by radiotracer technique; the insert shows detail of the data at the sulfate–methane transition (SMT); (H) sulfate reduction data from frame (G) in double logarithmic plot; line shows log-log linear correlation calculated without using elevated rates in the SMT; (I) cumulative rates of sulfate reduction integrated from the sediment surface to the bottom of the sulfate zone; the two axes indicate cumulative SRR in absolute rates and in percentage of total, respectively; additional AOM-driven SRR is indicated at the bottom of the SRR zone. Curves shown in (A), (B), and (D) are fitted with the PROFILE model and were used to calculate modeled rates in panel C.

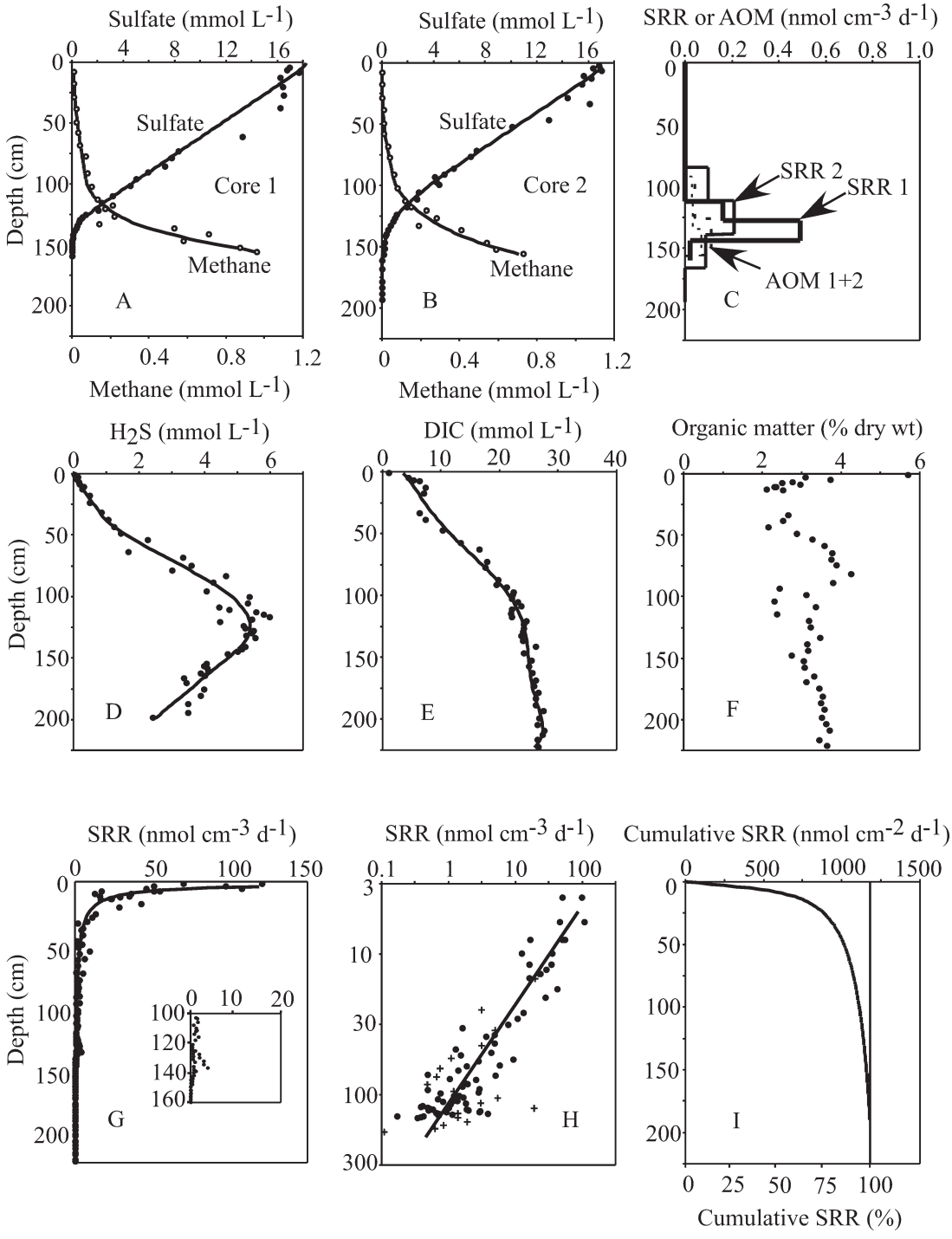

Fig. 3. Data from Sta. 2, Livø Strait. Legend: *see* Fig. 2. (G) AOM-driven SRR could not be discerned; (H) crosses show additional data from Jørgensen (1977).

the sediment and the DIC diffuses up according to a combination of their concentration gradients and their different diffusion coefficients, the diffusive fluxes of both were compared by multiplying the parameter slopes by the ratio between their molecular diffusion coefficients. Thus, the ratio in diffusion fluxes of DIC vs. sulfate was for Bjørnsholm Bay $1.66 \times (0.81/0.74) = 1.82$, and for Livø Strait = 1.30 (the diffusion coefficients are given in the Methods section).

Similar plots were made for H_2S vs. sulfate for the two stations (Fig. 4C,D). The slopes were -0.26 ($r^2 = 0.94$) for Bjørnsholm Bay and -0.31 ($r^2 = 0.95$) for Livø Strait.

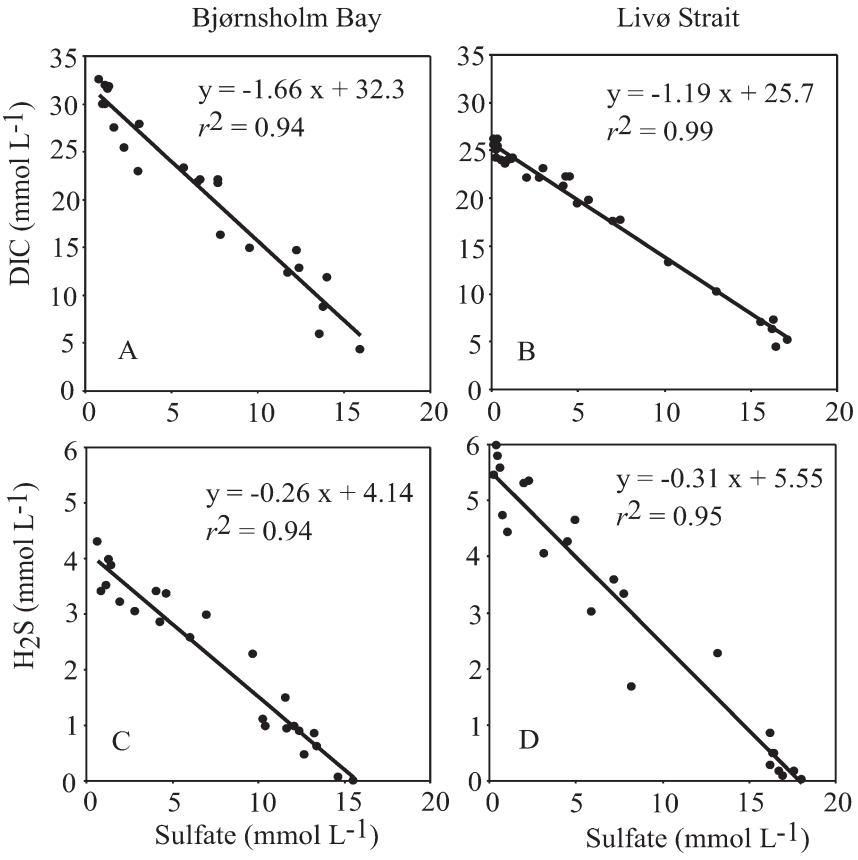

Fig. 4. Parameter plots of pore-water data from Bjørnsholm Bay (A, C) and Livø Strait (B, D). (A, B) show the relationship between DIC and sulfate concentrations, and (C, D) show the relationship between H_2S and sulfate. The linear regression equations and the r^2 values are shown.

Correspondingly, the flux ratios between H_2S and sulfate were 0.26 × (1.36/0.74) = 0.48 for Bjørnsholm Bay and 0.57 for Livø Strait.

Acetate and methane turnover—At Sta. 3, the acetate concentrations scattered between 2 and 5 μmol L^{-1} within the sulfate zone and increased slightly to 3–7 μmol L^{-1} in the methane zone (Fig. 5A). The ^{14}C-acetate oxidation rates dropped from 7 nmol cm^{-3} d^{-1} at the sediment surface to ca. 1 nmol cm^{-3} d^{-1} at the SMT (Fig. 5B). These rates corresponded well to the measured SRR in the lower half of the sulfate zone, whereas the rates were 2–10-fold lower than the SRR in the upper half. These potentially underestimated rates might be due to the considerable ^{14}C-acetate removal during incubation in the active near-surface layers (only ~ 10% ^{14}C-acetate remaining after incubation in the top 50 cm, compared to 70% in the sediments below).

Methanogenesis from ^{14}C-acetate was detectable only in the methane zone below 150-cm depth (Fig. 5C). Maximum rates of aceticlastic methanogenesis were 0.34 nmol cm^{-3} d^{-1}, about 10-fold lower than maximum rates of methanogenesis from CO_2 (Fig. 5D). Methanogenesis from $^{14}CO_2$ took place mostly below the SMT but was also detected at low rates (~ 0.3 nmol cm^{-3} d^{-1}) within the sulfate zone where methane tailing occurred (Fig. 5D).

At Sta. 2, the acetate concentrations were mostly scattered between 2 and 5 μmol L^{-1} but showed elevated concentrations up to 10 μmol L^{-1} at 20-cm depth and at the SMT (Fig. 5E). Rates of acetate oxidation to CO_2 followed the same trend as sulfate reduction but at lower rates (Fig. 5F). Methanogenesis from acetate was not detectable in the sulfate zone but took place in the entire methane zone, albeit at low rates (maximum 0.07 nmol cm^{-3} d^{-1}; Fig. 5G). Methanogenesis from CO_2 occurred at low rates throughout the core but still at rates up to six times higher than for aceticlastic methanogenesis. Surprisingly, there were distinctly elevated rates just above the SMT (Fig. 5H).

Discussion

Depth trend of SRRs—Sulfate reduction measured by radiotracer technique showed highest rates, > 100 nmol cm^{-3} d^{-1}, in the uppermost 5 cm. Such rates are typical for organic-rich, muddy sediments in eutrophic coastal environments where electron acceptors of higher energy yield, such as O_2, NO_3^-, Mn(IV), or Fe(III), may be largely exhausted within the uppermost few centimeters of the sediment (Thamdrup 2000). Below 5 cm the measured SRR decreased steeply. Rates could be described by a log-log linear decrease with depth at both stations (Figs. 2H, 3H),

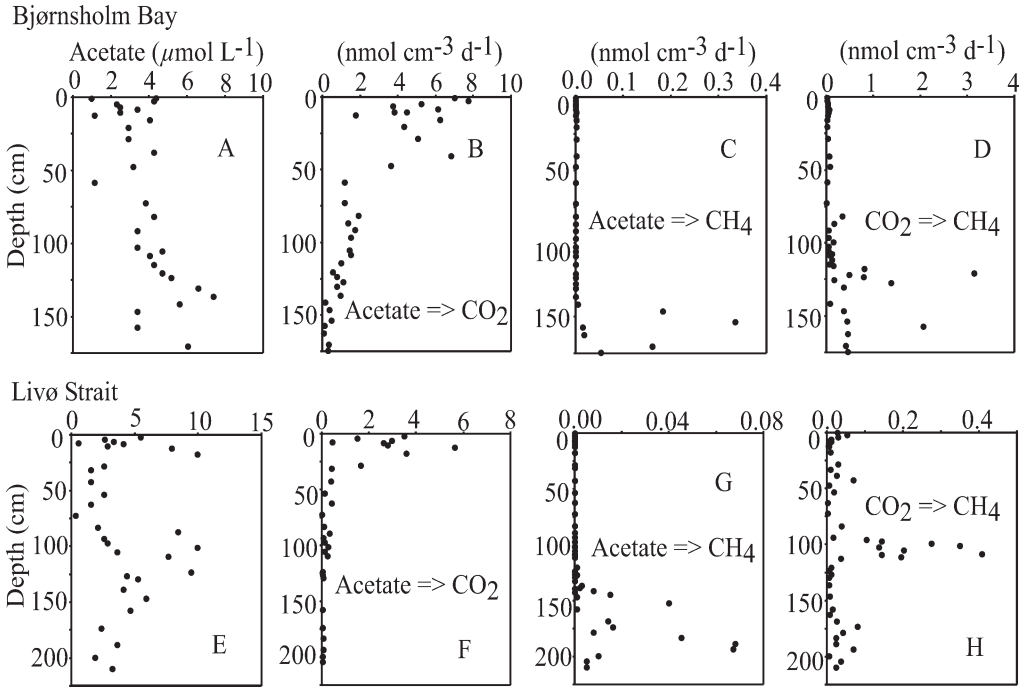

Fig. 5. Data from (A–D) Bjørnsholm Bay and (E–H) Livø Strait. (A, E) Acetate concentrations in pore water; (B, F) ^{14}C-acetate oxidation to CO_2; (C, G) methanogenesis from ^{14}C-acetate; (D, H) methanogenesis from $^{14}CO_2$.

with relatively less scatter of the rates around the linear correlation line at Sta. 3 than at Sta. 2.

A variation of experimentally measured SRRs according to a power law function of depth, and thus age, in the sediment has also been observed in other sediments (Jørgensen 1978*b*; L. Holmkvist unpubl.; K. Lettmann unpubl.). This is in accordance with the log-log linear relationship found between the age of marine organic material and its degradation rate constant (Middelburg 1989). Middelburg found an exponent of −1 for a very broad time window of ages of the organic matter, ranging from 1 d to 1 million yr. We found here exponents of −1.42 and −1.69 in Limfjorden for experimentally measured SRRs vs. depth. Similar exponents for other marine sediments range from −1 to −3, with most values between −1 and −2 (K. Lettmann unpubl.). The more negative exponents of −2 to −3 imply a large span of degradation rate constants for different organic carbon pools buried below the sediment surface. Thus, relatively rapid degradation of fresh organic matter takes place near the sediment surface whereas organic matter buried at depth is very refractory. Conversely, a less negative exponent of −1 would imply smaller differences in degradation rate constants between the upper and the deeper sediment layers. In the latter case, the organic matter may have undergone more extensive degradation in the bioturbated zone near the sediment surface before it is buried in the sulfate reduction zone.

As a conceptual model, the depth trend of organic carbon degradation may be considered to be the sum of mineralization rates for many initial pools, ΣG_i, of organic material, each decaying exponentially with time and depth. Such a "multi-G" concept, first developed by Jørgensen (1978*b*) and Westrich and Berner (1984), was generalized into a reactive continuum model by Boudreau and Ruddick (1991). It can be shown that the reactive continuum model approaches a power law function when fitted to experimentally measured SRR data, such as those from Limfjorden (Tarutis 1993; K. Lettmann unpubl.). Thus, in the depth interval from 10-cm sediment depth to the bottom of the sulfate zone at 120 cm at Sta. 3, the best fits of the reactive continuum model and of the power law function provided SRR distributions that largely coincided and showed a maximum difference of 17% (Fig. 6A). In contrast to the reactive continuum model, the power law function does not have a conceptual background in the mechanism or kinetics of organic matter degradation. It is just a simple function that, at least for the Limfjorden data and several other data sets, describes the observations equally as well as the conceptually more correct reactive continuum model.

SRRs modeled from the reaction-transport model, PROFILE, of Berg et al. (1998), assuming transport only by molecular diffusion, showed very low or even no sulfate reduction down through most of the sulfate zone (Figs. 2C, 3C). Thus, at mid-depth in the sulfate zone of Sta. 3, for example at 50 cm, modeled rates were > 30-fold below the mean ^{35}S-measured rates. The discrepancy could be due to the modeled rates being too low, for example because of a reoxidation of sulfide by buried Fe(III), which may have a similar low reaction rate constant to that of the organic material (Canfield et al. 1992). It can be shown, however, that such a reoxidation in combination with a quantitative binding of the formed Fe(II) as pyrite in the subsurface sediment can convert only a small fraction, less than 10%, of the sulfide back into sulfate (L. Holmkvist unpubl.). Introduction of oxygen at depth due to deep bioirrigation

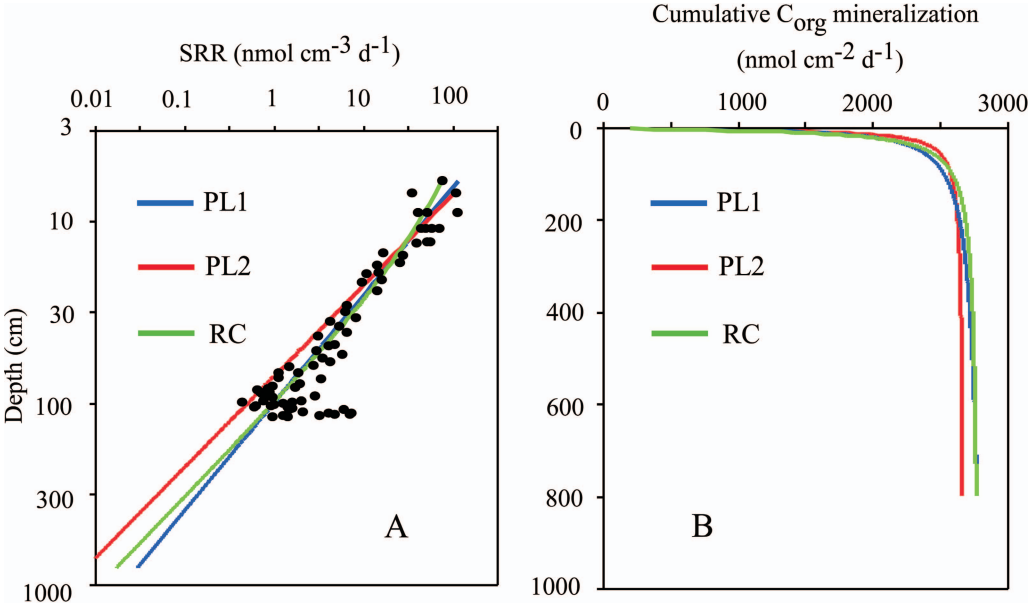

Fig. 6. (A) Log-log plot of sulfate reduction rates in sediment from Sta. 3, Bjørnsholm Bay. Data points show SRR measured by the ^{35}S method. The blue line (PL1) shows a linear correlation to the log-log data (calculated without the enhanced AOM-driven SRR). The red line (PL2) shows a similar power law function that is based on the low SRR data and that better fits the methane flux. The green line (RC) shows the best fit using a reactive continuum model. (B) Depth-integrated rates of organic carbon mineralization from sulfate reduction, accumulated from the sediment surface to the different subsurface depths. Color codes as in A.

might, however, cause a more extensive oxidation of sulfide to sulfate, a process that could not be quantified here.

The modeled SRR may also be too low because transport not only is due to molecular diffusion but is enhanced by bioirrigation from burrowing fauna (see below).

Role of methane for sulfate reduction—The experimental ^{35}S data on sulfate reduction throughout the sulfate zone allows a depth-integrated calculation of sulfate reduction and a comparison of how much of the entire sulfate reduction was driven by methane relative to the methane-independent sulfate reduction ("non-AOM" SRR). In the following, we will first discuss data from Bjørnsholm Bay.

By the depth integration of ^{35}S-determined SRR, we used the mean measured rates in the upper 0–5 cm of 95 nmol cm^{-3} d^{-1}. From 5-cm depth to the bottom of the sulfate zone at 120 cm, the log-log linear correlation shown in Fig. 2H was used to calculate a total depth-integrated rate of 12.80 mmol m^{-2} d^{-1} (Table 2). The mean AOM-derived peak of SRR detected in the SMT at 100–120-cm depth (Fig. 2G) was 1.5 nmol cm^{-3} d^{-1}, which, when integrated over the 20-cm depth interval of the AOM zone, results in an areal rate of 0.30 mmol m^{-2} d^{-1} (Table 2). Thus, according to the ^{35}S-determined rates, the total areal rate of SRR in the sediment column was 13.10 mmol m^{-2} d^{-1}. Only ((0.30 × 100)/13.10 =) 2.3% of this total SRR was apparently driven by methane. This small contribution of AOM-driven SRR is seen as a deviation from a smooth profile from 100- to 120-cm depth (Fig. 2I, arrow).

Diffusion-reaction modeling of sulfate reduction based on measured pore-water sulfate provided a smooth fit to the data in the deep part of the sulfate zone (Fig. 2A,B). For both Core 1 and Core 2, the model calculates enhanced SRR of 0.2–0.5 nmol cm^{-3} d^{-1} at the SMT (Fig. 2C), which we interpret as AOM-driven sulfate reduction. By integrating these modeled rates over the depth intervals of enhanced SRR, a mean AOM-driven SRR of 0.184 mmol m^{-2} d^{-1} is calculated (Table 2). This is 60% of the AOM-driven SRR calculated from the ^{35}S-SRR data.

Similar modeling of AOM can be done based on the methane profiles, which provide a mean areal AOM rate of 0.076 mmol CH_4 m^{-2} d^{-1} (Table 2, mean of cores 1 + 2).

Table 2. Sulfate reduction rates (mmol m^{-2} d^{-1}) determined from ^{35}S experiments compared to modeled rates of AOM-driven SRR, AOM, and H_2S fluxes.*

Process	Core	3. Bjørnsholm Bay	2. Livø Strait
Radiotracer measurements			
Total non-AOM SRR	1+2	12.80	11.9
AOM-driven SRR	1+2	0.30	n.d.
Modeling			
AOM-driven SRR	1	0.184	0.107
	2	0.183	0.108
	1+2	0.184	0.108
AOM	1	0.074	0.046
	2	0.078	0.028
	1+2	0.076	0.037
H_2S net production	1	0.291	0.290
H_2S flux upwards	1	0.186	0.040†
H_2S flux downwards	1	0.105	0.187

* n.d., not detectable.
† Part of the upwards H_2S flux was consumed subsurface.

Because the net reaction of methane oxidation with sulfate requires a 1 : 1 stoichiometry (Nauhaus et al. 2002), this is only 40% of the modeled, presumably AOM-driven, SRR:

$$CH_4 + SO_4^{2-} \rightarrow HCO_3^- + HS^- + H_2O \quad (4)$$

Because the two modeled rates are based on pore-water gradients measured pair-wise in the same core, a better agreement might be expected. A comprehensive analysis of sulfate and methane data from the literature has shown, however, that calculated methane fluxes into the SMT are most often lower than the corresponding sulfate flux into the SMT and that the modeled AOM is, thus, generally lower than the total SRR within the SMT (N. Riedinger unpubl.). Sulfate reduction based on organic matter remineralization can occur in the SMT, but other factors may also contribute to this difference, and will not be discussed further here. Because both sulfate and methane gradients are analyzed in the same cores, their diffusion fluxes must be affected by similar physical properties, such as turtuosity or temperature, so that the ratio of their whole-sediment diffusion coefficients can be assumed to be similar to the ratio of their molecular diffusion coefficients, which are taken from the literature. The ratio of the whole-sediment diffusion coefficients of sulfate and methane has also been checked by experimental determination of their diffusion coefficients in sediments similar to those of Limfjorden using $^{35}SO_4^{2-}$ and $^{14}CH_4$ (Iversen and Jørgensen 1993).

Modeled H_2S production—The product of dissimilatory sulfate reduction is H_2S, which reached peak concentration in the pore water at the SMT depth (Fig. 2D). By modeling the pore-water H_2S data, assuming molecular diffusion only, a total areal H_2S production of 0.291 mmol m^{-2} d^{-1} was calculated (Table 2). This happens to be similar to the ^{35}S-measured AOM-driven SRR (0.30 mmol m^{-2} d^{-1}), but it is little more than 2% of the total ^{35}S-measured SRR. Thus, as with modeling of sulfate removal, the modeling of H_2S production underestimates the measured gross rate of sulfate reduction, probably because of an underestimation of the transport coefficient. Furthermore, the net H_2S production is lower than its modeled production from sulfate reduction because of the precipitation of sulfide and binding in iron sulfides, especially in pyrite, which is by far the predominant iron sulfide mineral (Jørgensen 1978*c*). The ratio between upwards H_2S flux and downwards sulfate flux through the sulfate zone was 0.48 and 0.57 for the two stations, which also shows that much of the produced H_2S was trapped within the subsurface sediment. Interestingly, out of the modeled net production of H_2S, two thirds diffused up towards the sediment surface whereas one third diffused down (Table 2), presumably to be trapped by excess reactive iron at a deep sulfidization front.

Similar calculations for the Livø Strait station show a very similar total areal SRR of 11.9 mmol m^{-2} d^{-1} (Table 2). Because of scatter of the ^{35}S-determined SRRs (Fig. 3H), we could barely distinguish an AOM-driven SRR above the general depth trend of SRR. The mean areal SRR in the AOM zone was, based on diffusion-reaction modeling, 0.108 mmol SO_4^{2-} m^{-2} d^{-1} (Table 2), whereas the mean modeled AOM, based on the CH_4 profile, was only one third of this, 0.037 mmol CH_4 m^{-2} d^{-1}. The net H_2S production was similar to that at the Bjørnsholm Bay station, but a larger fraction of the H_2S diffused downwards rather than upwards, assuming molecular diffusion only.

Organic matter degradation by sulfate reduction or methane production—The measured depth variation of organic carbon mineralization through sulfate reduction could be described by a simple power law function of depth: $SRR = A \times z^{-b}$ where A is the extrapolated rate for z = 1-cm depth, whereas the exponent −b defines how steeply the SRR decreases with depth, z (cf. Eq. 2). Because the rate-limiting step in anaerobic carbon mineralization is generally the initial enzymatic attack on polymeric organic material, the depth trend of organic carbon mineralization observed from SRR data should not be specific to the sulfate zone but may continue down into the methane zone. In the following we make an extrapolation of the mineralization trend from the sulfate zone and down into the methane zone in order to evaluate the consequences of the calculated power law function under presumed steady-state conditions. Thus, we calculate the total extrapolated mineralization rate and compare this with the burial rate of organic matter down into the methane zone. Furthermore, we take the extrapolated rate of conversion of buried organic matter into methane and compare this with the return flux of methane up to the SMT. This exercise requires information about the geological history and burial rate of the sediment and will assume that the depth distributions of chemistry and process rates are currently in quasi-steady state.

Kristensen et al. (1995) and Christensen et al. (2004) analyzed the late Holocene development of Limfjorden based on biostratigraphic studies of a 5.3-m-deep sediment core from Sta. 3 in Bjørnsholm Bay. Sediment below 200-cm depth had a marine benthic fauna typical of salinities above 30, and also the dinoflagellate species found as cysts indicated fully marine conditions. At 200 cm, where ^{14}C dating of shells from mollusks and foraminifera indicated an age of 2000–2500 yr, Limfjorden changed to brackish conditions with an estimated salinity of 7–15. More recent deposits between 135- and 0-cm depth showed alternating marine and brackish conditions related to the opening and closing of connections between Limfjorden and the North Sea. Thus, the recurrence of a marine period around 100-cm depth took place ca. 1000 yr ago based on the ^{14}C age, which is in accordance with geological data and with historical reports of navigation by the Vikings from Limfjorden and directly out to the Skagerrak, located at the transition between the North Sea and the Baltic Sea (Fig. 1). Based on this chronology, the mean sediment accumulation rate over the past 2000 yr has been 1 mm yr^{-1}. The most recent sediment at 0–33-cm depth has apparently been deposited since the last reopening of the connection to the North Sea by a storm in 1825, which leads to a higher mean sedimentation rate of ca. 2 mm yr^{-1}. This surface

Table 3. Carbon budget for the mineralization of organic matter buried in the sediment of Sta. 3 in Bjørnsholm Bay. The model calculations are based on ^{35}S-determined SRR and a comparison of extrapolated CH_4 production with CH_4 flux up into the SMT. Model PL1 is a power law function calculated from linear regression of log ^{35}S-SRR vs. log depth. Model PL2 is a similar power law function calculated from the low ^{35}S-SRR data. Model RC is based on a reactive continuum model fit to the measured ^{35}S-SRR data, similar to PL1.

Depth interval	Model PL1	Model PL2	Model RC
Cumulative carbon mineralization rate (nmol C_{org} cm^{-2} d^{-1})			
0–33 cm	2220	2380	2250
33–120 cm	340	220	370
120–800 cm	210	70	150
Total, 0–800 cm	2770	2670	2770
Depth-integrated organic carbon mineralization (mmol C_{org} cm^{-3})			
0–33 cm	4.04	4.35	4.11
33–120 cm	1.26	0.79	1.35
120–800 cm	0.76	0.25	0.55
Total, 0–800 cm	6.06	5.39	6.01

sedimentation rate is similar to the rate estimated by Jørgensen (1977). A sedimentation rate of about 2 mm yr^{-1} has since then been confirmed by ^{210}Pb dating for a nearby area of Limfjorden (Christiansen et al. 2006). The porosity of the sediment decreased from 0.78 at the surface to ca. 0.57 at 33 cm. This corresponds to a gradual compaction of the sediment by a factor of nearly two, which at constant deposition rate could account for the decrease in the calculated sediment accumulation rate with depth.

As stated above, an important consideration for the following calculations is that a change in mineralization rate of organic matter with age is independent of whether the sediment is situated within the sulfate zone or within the methane zone. We assume that the variations in salinity in Limfjorden over the past several thousand years, and thus the variations in the surface concentration and penetration depth of sulfate, have not controlled the mineralization rates at depth. These have been controlled rather by the amount and inherent degradability of the buried organic matter, irrespective of varying salinity and whether the terminal process was sulfate reduction or methanogenesis.

The pore-water profiles adjust relatively fast to variations in salinity, as the following calculation shows (Jørgensen et al. 2001). The mean diffusion time (t) of sulfate from the overlying seawater and down to the present SMT at 120 cm can be calculated from $t = \pi L^2/4D_s$, where L is the diffusion distance (120 cm) and D_S is the mean whole-sediment diffusion coefficient at the annual mean temperature of 9°C ($D_{sulfate} = 0.66 \times 10^{-5}$ cm^2 s^{-1}). The diffusion time is thus $(((3.14 \times 120^2)/(4 \times (0.66 \times 10^{-5})/(1 + 3(1-0.57))) \times 60 \times 60 \times 24 \times 365) = 125$ yr. This is relatively fast compared to the past Holocene variations in salinity over thousands of years. It is also shorter than the nearly 200 yr that have passed since the last opening of Limfjorden to the North Sea. Thus, pore-water gradients are the result of the modern mineralization rates rather than those of the past Holocene history of Limfjorden.

We first use the log-log linear correlation of ^{35}S-determined SRR vs. depth at the Bjørnsholm Bay Station ($SRR = 2320 \times z^{-1.69}$ nmol cm^{-3} d^{-1}) to calculate the organic carbon mineralization in the sulfate zone (Fig. 6A, blue line PL1). This correlation line is named PL1 for power law function No. 1. In the depth interval with ca. 2 mm sedimentation per year, from the sediment surface to 33-cm depth, the depth-integrated SRR is 1110 nmol SO_4^{2-} cm^{-2} d^{-1}, corresponding to an organic carbon oxidation of 2220 nmol C_{org} cm^{-2} d^{-1} (Table 3). In a coordinate system fixed at the sediment surface, the sediment moves downwards at 2 mm yr^{-1} in this interval because of sedimentation on the top, and the sediment thus spends on average 5 yr or 5×365 d in each 1-cm interval. The depth-integrated organic carbon mineralization at steady state from 0- to 33-cm depth is thus $2220 \times 5 \times 365 = 4.04 \times 10^6$ nmol C_{org} cm^{-3} or 4.04 mmol C_{org} cm^{-3} (Table 3). A similar calculation from 33 cm down to the bottom of the sulfate zone at 120-cm depth using a mean sediment burial rate of 1 mm per year yields an additional mineralization of 1.26 mmol C_{org} cm^{-3}. The base of the Holocene organic-rich mud deposit is, according to the sediment ages quoted above, predicted to be at 800 cm. Below that depth we expect postglacial silt and glacial till with very low organic content and thus insignificant methanogenesis. If the power law trend of organic carbon degradation rate vs. depth is extrapolated down to this base, an additional 0.76 mmol C_{org} cm^{-3} is mineralized in the methane zone below 120 cm, corresponding to 13% of the current anaerobic mineralization of organic carbon in the entire Holocene sediment.

The current burial rate of organic carbon below 120 cm can be estimated from the mean content of organic matter around that depth, 8% dry weight, as estimated from the ignition loss (Fig. 2F). The mean sediment dry weight at around that depth was 0.90 g cm^{-3}. The mean organic carbon content is thus ca. 2.4 mmol C_{org} cm^{-3}, as calculated from the dry weight of sediment per volume and assuming an organic matter composition of $[CH_2O]$. The extrapolated mineralization of organic carbon throughout the Holocene methane zone thus accounts for $0.76 \times 100/2.4 = 32\%$ of the organic carbon buried in that zone, which appears to be realistic. Data are not available to show how the organic carbon content actually changes in the deeper Holocene sediment.

The current cumulative mineralization rate of organic carbon, as extrapolated from the ^{35}S-determined SRR, was estimated to be 210 nmol C_{org} cm^{-2} d^{-1} in the methane zone from 120 to 800 cm (Table 3). If we assume that the conversion of organic matter into methane has the simple stoichiometry of

$$2[CH_2O] + H_2O \rightarrow CH_4 + HCO_3^- + H^+ \qquad (5)$$

then a total of 210/2 = 105 nmol CH_4 cm^{-2} d^{-1} or 1.05 mmol CH_4 m^{-2} d^{-1} should be produced in the Holocene sediment. The modeled CH_4 flux up to the SMT was only 0.076 mmol CH_4 m^{-2} d^{-1} (Table 2) or 7% of the total extrapolated CH_4 production.

Constraining calculated mineralization rates—There may be several reasons for this difference, including (1) only a fraction of the CH_4 produced in the methanogenic sediment makes it up to the SMT while a part of it accumulates as gas or is lost to deeper, low-methane deposits; (2) rates of organic carbon mineralization in the methanogenic sediment do not follow the power law function fitted for ^{35}S-determined mineralization rates in the sulfate zone, or (3) the depth trend of organic carbon mineralization may indeed follow an extrapolated power law function but the ^{35}S-determined rates in the lower sulfate zone are overestimated.

If (3) is correct then we can tentatively make an alternative extrapolation fitted to the low data points among measured non-AOM SRR ($SRR = 5000 \times z^{-2.00}$; red line PL2 in Fig. 6A). The total cumulative C_{org} mineralization in the methane zone would then decrease from 210 to 70 nmol C_{org} cm^{-2} d^{-1} (Table 3; Fig. 6B, red line PL2). This would yield a total methane production in the Holocene methane zone of 70/2 = 35 nmol CH_4 cm^{-2} d^{-1} or 0.35 mmol CH_4 m^{-2} d^{-1}. The modeled CH_4 flux is still only ($0.076 \times 100/0.35 =$) 22% of this production. Yet the modeled AOM-driven SRR would correspond to ($0.184 \times 100/0.35 =$) 53%. This extrapolation would imply the mineralization of 0.25 mmol C_{org} cm^{-3} in the methane zone, which is only 19% of the organic carbon currently buried in this zone. Thus, there should be sufficient organic carbon buried to account for such a mineralization.

These calculations were done also for a third fit to the measured SRR data using the reactive continuum model. Figure 6A (green line RC) shows that the modeled rates extrapolated down into the methane zone followed parallel to the low-rate power law line PL2 trend. The depth-integrated mineralization rates were 4.11 mmol C_{org} cm^{-3} in the 0–33-cm interval, 1.35 mmol C_{org} cm^{-3} in the sulfate zone from 33 to 120 cm, and 0.55 mmol C_{org} cm^{-3} in the methane zone down to 800 cm (Table 3). The total depth-integrated organic carbon mineralization throughout the Holocene sediment was about 6 mmol C_{org} cm^{-3}, irrespective of whether model PL1, PL2, or PL3 was used to simulate the ^{35}S-measured SRR (Fig. 6B; Table 3).

This exercise with numbers can be only a guideline to evaluate whether the experimental rate measurements and the model calculations are compatible with available information on organic carbon burial and age structure of the sediments. A main conclusion is that a depth trend of organic carbon mineralization corresponding to the low values of ^{35}S-measured SRR is compatible with the constraints provided by burial rates of C_{org} and with the calculated AOM rates. It is unlikely that mineralization rates in the sulfate zone are much lower than the low ^{35}S-SRR values, because the modeled depth trend must provide sufficient C_{org} mineralization to feed the CH_4 flux from below. Considering the general trend of degradability of organic matter according to a power law function with age (Middelburg 1989), it is also unlikely that there is no or barely any mineralization throughout the sulfate zone and then a step-up in mineralization rate in the methane zone. From this we conclude that the net SRRs modeled from pore-water sulfate, assuming only molecular diffusion and no reoxidation to sulfate (Figs. 2C, 3C), are unrealistic as they predict near-zero mineralization throughout most of the sulfate zone. The most likely scenario is that the mineralization rate of buried organic matter undergoes a continuous decrease with depth and age throughout the sulfate and methane zones.

Bioirrigation and sulfate reduction modeling—A modeling result that would take bioirrigation and bioturbation, i.e., pore-water advection and sediment mixing, due to the abundant benthic fauna into account would provide higher modeled rates, in particular near the sediment surface.

We modeled the depth distribution of biodiffusion coefficients that would reconcile measured and modeled SRR. The calculation was based on the equation for calculating the flux, J, of sulfate:

$$J = \phi D_s \, dC/dz \tag{6}$$

which by rearranging becomes

$$D_s = J/(\phi \, dC/dz) \tag{7}$$

For the calculations we used the low power law function, PL2, of SRR shown in Fig. 6A, including the AOM given in Table 2. This provided the depth-integrated gross SRR, which took place below each depth and which was equal to the flux, J, down through that depth horizon. Porosity was determined from a smooth fit to the measured values. The sulfate gradient was determined from the best fit to the measured sulfate data as calculated by the Berg model, PROFILE (e.g., Fig. 2A). Figure 7 shows for the two cores the depth distribution of the combined whole-sediment diffusion coefficient, which includes the molecular diffusion coefficient plus the additional biodiffusion coefficient. For comparison, the pure molecular diffusion coefficient (red curve) is also shown.

As shown in Fig. 7, the combined whole-sediment diffusion coefficient was $10–20 \times 10^{-5}$ cm^2 s^{-1} near the sediment surface. This was 25–50-fold higher than the corresponding molecular whole-sediment diffusion coefficient, 0.44×10^{-5} cm^2 s^{-1}. The combined whole-sediment diffusion coefficient dropped steeply with depth and was 2×10^{-5} cm^2 s^{-1} at 30-cm depth. It was near the molecular diffusion coefficient from 60-cm depth.

The question is whether bioirrigation from deeply burrowing polychaetes, bivalves, or other fauna could have an effect down to 30 cm or even 60 cm. Bioirrigation was not directly quantified, but burrowing macrofauna causing bioirrigation and bioturbation were abundant in the Limfjorden sediments. An annual bottom fauna survey carried out since 1978 as part of the environmental monitoring program by the Limfjorden Committee in the nearby Løgstør Broad showed a very high total biomass of 500–1000 g fresh weight m^{-2}. The mean density of polychaetes was 800 individuals m^{-2}, of which the species *Nephtys hombergii* and *Nereis diversicolor* were particularly abundant. Both species cause bioturbation and intense bioirrigation down to at least 20–30-cm depth in sediments (Schöttler 1982; Davey 1993; Koretsky et al. 2002). In the very

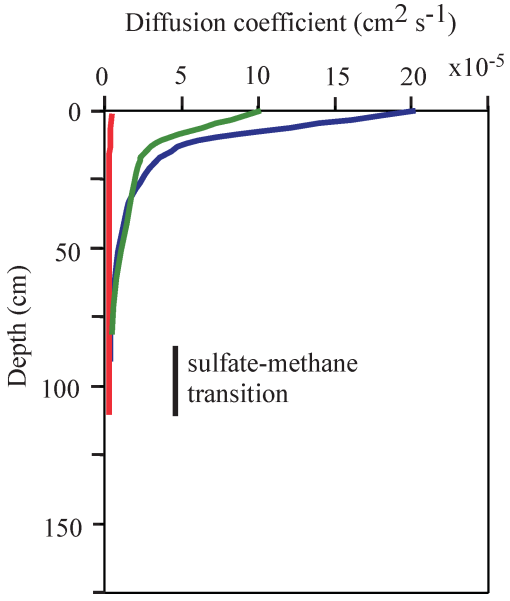

Fig. 7. Modeled diffusion coefficients in the sediment of Sta. 3, Bjørnsholm Bay. The blue (Core 1) and green (Core 2) curves show total molecular plus biodiffusion coefficients required to match the modeled and the measured SRR. The red curve shows the corresponding molecular diffusion coefficient.

similar sediments of Aarhus Bay, Denmark, bioirrigation caused an enhanced biodiffusion coefficient, which dropped over the top 7 cm from 5000 to 1000×10^{-5} cm^2 s^{-1}, i.e., 10^3–10^4 times higher than the molecular diffusion coefficient of sulfate (Thamdrup et al. 1994) and ca. 100 times higher than the biodiffusion coefficient calculated for the same depth interval of Limfjorden sediment.

The benthic polychaetes pump water down into their burrow tubes for respiration and feeding. It takes very little of such nonlocal transport of seawater sulfate down into the sediment to cover the entire underlying sulfate consumption. For example, to transport sufficient seawater sulfate down to 30-cm depth and cover all measured sulfate reduction below 30 cm (power law function P2) would require that 1 out of 10 polychaetes pump 1 mL of seawater to that depth per day, which is a minute fraction of their normal pumping rates.

Stoichiometry of mineralization—The downwards diffusion flux of sulfate from the sediment surface to the bottom of the sulfate zone should be mirrored stoichiometrically by an upwards DIC flux. The flux ratios of DIC to sulfate should be 2 : 1 according to the simple stoichiometry used above:

$$2[CH_2O] + SO_4^{2-} \rightarrow 2HCO_3^- + HS^- + H^+ \qquad (8)$$

The flux ratio should also be 2 : 1 for the deeper fraction of organic carbon mineralized by methanogenesis (Eq. 5), provided that the methane was subsequently oxidized with sulfate at the SMT (the sum of Eqs. 5 and 4 is equal to Eq. 8). The flux ratios of DIC : sulfate were only 1.82 for Bjørnsholm Bay and 1.30 for Livø Strait. This indicates that the organic matter being mineralized is more reduced than the carbohydrate assumed in Eq. 8, which is also in accordance with several other studies. For example, Alperin et al. (1994) found a ratio of DIC production to sulfate reduction of 1.7 : 1 in incubation experiments with coastal marine sediment from Cape Lookout Bight. Such a stoichiometry will slightly change the carbon budget calculations made above. The low DIC : sulfate ratio could also be due to a concurrent loss of DIC, possibly by precipitation as carbonate. Pore-water data for Ca^{2+} or Mg^{2+} ions are not available to calculate the rate of carbonate precipitation as a DIC sink.

Similarly, the depth-integrated methane production below the SMT should result in an equivalent production of DIC, according to Eq. 5. The upwards flux of DIC to the SMT was difficult to estimate at the Bjørnsholm Bay station because of data scatter and the irregular shape of the DIC gradient (Fig. 2E). At the Livø Strait station the DIC profile showed a distinct break at the SMT (Fig. 3E). The upwards flux of DIC from the methane zone, calculated as HCO_3^- diffusion, was estimated to be 0.081 mmol m^{-2} d^{-1}, which is about twice the upwards flux of methane (Table 2). Thus, carbonate dissolution might currently take place in the deep methane zone. Alternatively, the methane fluxes may be underestimated, possibly because of a loss of methane during sampling in spite of great efforts to prevent such a loss.

Acetate turnover and methanogenesis—Acetate was detected in the pore water at both stations at concentrations ranging from 1 to 10 μmol L^{-1}, with generally higher concentrations in the methane zone than in the sulfate zone (Fig. 5). The oxidation rates of ^{14}C-acetate to $^{14}CO_2$ followed the depth trend of sulfate reduction but at much lower rates in the upper part of the sulfate zone, where the estimated turnover time of pore-water acetate was half a day, as calculated from the ^{14}C data. A comparison with the ^{35}S-measured SRR of ca. 100 nmol cm^{-3} d^{-1} in the top 5 cm, however, leads to turnover times of only 1–2 h, assuming that acetate, as a mean value of literature data, comprises half to two thirds of the electron donor requirement for sulfate reduction (Sørensen et al. 1981; Parkes et al. 1989).

Extrapolation of SRR activity from the PL2 model in Fig. 5A to the deeper sulfate-free zone suggested that the total methanogenesis should decrease from 0.3 to 0.1 nmol cm^{-3} d^{-1} between the SMT and down to ca. 200-cm depth. The ^{14}C-measured rates of methanogenesis from acetate or CO_2 scattered strongly but show that methanogenesis was predominantly from CO_2 (Fig. 5C,D). Overall rates of methanogenesis were mostly $\leq$ 0.5 nmol cm^{-3} d^{-1}, i.e., in a similar range to the rates predicted by extrapolation of the non-AOM ^{35}S-SRR data.

Experimental measurements of methanogenesis in sediment from Livø Strait showed a different but very distinct zonation. It was interesting that methanogenesis from CO_2 was detected throughout the sulfate zone with highest rates near the SMT, where there may be an enhanced methane cycling involving both the formation and the oxidation of methane (Parkes et al. 2007). Rates of methanogenesis

below the SMT and down to 210 cm were lower than in Bjørnsholm Bay, 0.01–0.04 nmol cm^{-3} d^{-1} from acetate and 0.02–0.1 nmol cm^{-3} d^{-1} from CO_2. Extrapolation of the non-AOM ^{35}S-SRR data into the methane zone, again using the lower data points, suggests similar mineralization rates. The experimental determinations of methanogenesis from acetate and CO_2 thus support the general conclusions concerning the continuous, gradual decrease in organic carbon mineralization down through the sulfate and methane zones.

Conclusion—In conclusion, the different results of experimental rate measurements of SRR and modeling of pore water and solid phase data converge when bioirrigation and bioturbation are considered in the modeling. The ^{35}S measurements of sulfate reduction appeared, in the present study, to overestimate the in situ rates in the deeper part of the sulfate zone. The microbial communities have here lived under relatively constant conditions for hundreds to thousands of years and may therefore react in a more sensitive way to the experimental manipulations than do communities in the bioturbated surface sediment.

Acknowledgments

We thank Kathryn Kuivila for radiotracer measurements of bicarbonate methanogenesis and analyses of dissolved inorganic carbon, Karsten Lettmann for providing reactive continuum model data, Niels Iversen for analyses of methane, and Hans Jensen (former skipper on R/V *Genetica*), Leon X. Zawacki, Preben G. Sørensen, Kathryn Kuivila, and Niels Iversen for assistance with sample collection and preparation. Stimulating discussions with Marc Alperin and recommendations by him and an anonymous reviewer helped to improve the manuscript. Financial support was provided by the Danish Natural Science Research Council (to B.B.J.) and by Dunstaffnage Marine Laboratory, UK (to R.J.P.).

References

Alperin, M. J., D. B. Albert, and C. S. Martens. 1994. Seasonal variations in production and consumption rates of dissolved organic carbon in an organic-rich coastal sediment. Geochim. Cosmochim. Acta **58:** 4909–4930, doi:10.1016/0016-7037(94)90221-6

Ansbæk, J., and T. H. Blackburn. 1980. A method for the analysis of acetate turnover in a coastal marine sediment. Microb. Ecol. **5:** 253–264, doi:10.1007/BF02020333

Berg, P., N. Risgaard-Petersen, and S. Rysgaard. 1998. Interpretation of measured concentration profiles in sediment pore water. Limnol. Oceanogr. **43:** 1500–1510.

Borowski, W. S., C. K. Paull, and W. Ussler, III. 1996. Marine pore-water sulfate profiles indicate in situ methane flux from underlying gas hydrate. Geology **24:** 655–658, doi:10.1130/0091-7613(1996)024<0655:MPWSPI>2.3.CO;2

———, ———, and ———. 1999. Global and local variations of interstitial sulfate gradients in deep-water, continental margin sediments: Sensitivity to underlying methane and gas hydrates. Mar. Geol. **159:** 131–154, doi:10.1016/S0025-3227(99)00004-3

Boudreau, P. B., and B. R. Ruddick. 1991. On the reactive continuum representation of organic matter diagenesis. Am. J. Sci. **291:** 507–538.

Canfield, D. E., R. Raiswell, and S. Bottrell. 1992. The reactivity of sedimentary iron minerals toward sulfide. Am. J. Sci. **292:** 659–683.

———, ———, J. T. Westrich, C. M. Reaves, and R. A. Berner. 1986. The use of chromium reduction in the analysis of reduced inorganic sulfur in sediments and shales. Chem. Geol. **54:** 149–155, doi:10.1016/0009-2541(86)90078-1

Christensen, J. T., T. Cedhagen, and J. Hylleberg. 2004. Late-Holocene salinity changes in Limfjorden, Denmark. Sarsia **89:** 379–387, doi:10.1080/00364820410002640

Christiansen, T., T. J. Christensen, S. Markager, J. K. Petersen, and L. T. Mouritsen. 2006. Limfjorden during 100 years. Climate, hydrography, nutrient influx, bottom fauna and fishes in Limfjorden from 1897 to 2003. Danmarks Miljøundersøgelser, Technical Report No. 578, Copenhagen, Denmark. [In Danish.]

Cline, J. D. 1969. Spectrophotometric determination of hydrogen sulfide in natural waters. Limnol. Oceanogr. **14:** 454–458.

Davey, J. T. 1993. Macrofaunal community bioturbation along an estuarine gradient. Aquat. Ecol. **27:** 147–153, doi:10.1007/BF02334777

Devol, A. H., J. J. Anderson, K. Kuivila, and J. W. Murray. 1984. A model for coupled sulfate reduction and methane oxidation in the sediments of Saanich Inlet. Geochim. Cosmochim. Acta **48:** 993–1004, doi:10.1016/0016-7037(84)90191-1

Fossing, H., and B. B. Jørgensen. 1989. Measurement of bacterial sulfate reduction in sediments. Evaluation of a single-step chromium reduction method. Biogeochemistry **8:** 205–222, doi:10.1007/BF00002889

Iversen, N., and B. B. Jørgensen. 1993. Diffusion coefficients of sulfate and methane in marine sediments: Influence of porosity. Geochim. Cosmochim. Acta **57:** 571–578, doi:10.1016/0016-7037(93)90368-7

Jørgensen, B. B. 1977. The sulfur cycle of a coastal marine sediment (Limfjorden, Denmark). Limnol. Oceanogr. **22:** 814–832.

———. 1978*a*. A comparison of methods for the quantification of bacterial sulfate reduction in coastal marine sediments. I. Measurement with radiotracer techniques. Geomicrobiol. J. **1:** 11–27, doi:10.1080/01490457809377721

———. 1978*b*. A comparison of methods for the quantification of bacterial sulfate reduction in coastal marine sediments. II. Calculation from mathematical models. Geomicrobiol. J. **1:** 29–47, doi:10.1080/01490457809377722

———. 1978*c*. A comparison of methods for the quantification of bacterial sulfate reduction in coastal marine sediments. III. Estimation from chemical and bacteriological field data. Geomicrobiol. J. **1:** 49–64, doi:10.1080/01490457809377723

———, A. Weber, and J. Zopfi. 2001. Sulfate reduction and anaerobic methane oxidation in Black Sea sediments. Deep-Sea Res. I **48:** 2097–2120, doi:10.1016/S0967-0637(01)00007-3

Kallmeyer, J., T. G. Ferdelman, A. Weber, H. Fossing, and B. B. Jørgensen. 2004. A cold chromium distillation procedure for radiolabeled sulfide applied to sulfate reduction measurements. Limnol. Oceanogr. Methods **2:** 171–180.

Kanneworff, E., and W. Nicolaisen. 1973. The "Haps," a frame supported bottom corer. Ophelia **10:** 119–128.

Koretsky, C. M., C. Meile, and P. van Cappellen. 2002. Quantifying bioirrigation using ecological parameters: A stochastic approach. Geochem. Trans. **3:** 17–30, doi:10.1186/1467-4866-3-17

Kristensen, P., S. Heier-Nielsen, and J. Hylleberg. 1995. Late-Holocene salinity fluctuations in Bjørnsholm Bay, Limfjorden, Denmark, as deduced from micro- and macrofossil analysis. Holocene **5:** 313–322, doi:10.1177/095968369500500306

KUIVILA, K. M., J. W. MURRAY, A. H. DEVOL, AND P. C. NOVELLI. 1989. Methane production, sulfate reduction and competition for substrates in the sediments of Lake Washington. Geochim. Cosmochim. Acta **53:** 409–416, doi:10.1016/0016-7037(89)90392-X

MIDDELBURG, J. J. 1989. A simple rate model for organic matter decomposition in marine sediments. Geochim. Cosmochim. Acta **53:** 1577–1581, doi:10.1016/0016-7037(89)90239-1

NAUHAUS, K., A. BOETIUS, M. KRÜGER, AND F. WIDDEL. 2002. In vitro demonstration of anaerobic oxidation of methane coupled to sulphate reduction in sediment from a marine gas hydrate area. Environ. Microbiol. **4:** 296–305, doi:10.1046/j.1462-2920.2002.00299.x

PARKES, R. J., G. R. GIBSON, I. MUELLER-HARVEY, W. J. BUKINGHAM, AND R. A. HERBERT. 1989. Determination of the substrates for sulphate-reducing bacteria within marine and estuarine sediments with different rates of sulphate reduction. J. Gen. Microbiol. **135:** 175–187.

———, AND J. TAYLOR. 1983. Analysis of volatile fatty acids by ion-exclusion chromatography, with special reference to marine pore water. Mar. Biol. **77:** 113–118, doi:10.1007/BF00396308

———, AND OTHERS. 2007. Biogeochemistry and biodiversity of methane cycling in subsurface marine sediments (Skagerrak, Denmark). Environ. Microbiol. **9:** 1146–1161, doi:10.1111/j.1462-2920.2006.01237.x

REEBURGH, W. S. 1967. An improved interstitial water sampler. Limnol. Oceanogr. **12:** 163–165.

SCHÖTTLER, U. 1982. An investigation on the anaerobic metabolism of *Nephtys hombergii* (Annelida: Polychaeta). Mar. Biol. **71:** 265–269, doi:10.1007/BF00397043

SCHULZ, H. D. 2006. Quantification of early diagenesis: Dissolved constituents in pore water and signals in the solid phase, p. 75–125. *In* H. D. Schulz and M. Zabel [eds.], Marine geochemistry. Springer.

SØRENSEN, J., D. CHRISTENSEN, AND B. B. JØRGENSEN. 1981. Volatile fatty acids and hydrogen as substrates for sulfate-reducing bacteria in anaerobic marine sediment. Appl. Environ. Microbiol. **42:** 5–11.

TARUTIS, W. J., JR. 1993. On the equivalence of the power and reactive continuum models of organic matter diagenesis. Geochim. Cosmochim. Acta **57:** 1349–1350.

THAMDRUP, B. 2000. Bacterial manganese and iron reduction in aquatic sediments. Adv. Microb. Ecol. **16:** 41–84.

———, H. FOSSING, AND B. B. JØRGENSEN. 1994. Manganese, iron, and sulfur cycling in a coastal marine sediment, Aarhus Bay, Denmark. Geochim. Cosmochim. Acta **58:** 5115–5129, doi:10.1016/0016-7037(94)90298-4

WESTRICH, J. T., AND R. A. BERNER. 1984. The role of sediment organic matter in bacterial sulfate reduction: The G-model tested. Limnol. Oceanogr. **29:** 236–249.

ZHABINA, N. N., AND I. VOLKOV. 1978. A method of determination of various sulfur compounds in sea sediments and rocks, p. 735–746. *In* W. E. Krumbein [ed.], Environmental biogeochemistry and geomicrobiology, v. 3. Ann Arbor Science.

Associate editor: Bo Thamdrup

Received: 08 June 2009
Accepted: 24 January 2010
Amended: 17 February 2010